Journal of the Korean Nuclear Society
Volume 30, Number 4, pp.328~341, August 1998

Turbulent Flow in an Axially Finned Rod Bundle with Spacer Grids

H. J. Chung, S. Cho, S. Y. Chun, S. K. Yang, and M. K. Chung

Korea Atomic Energy Research Institute
150 Dukjin-dong, Yusong-gu, Taejon 305-353, Korea

(Received December 1, 1997)

Abstract

This paper presents in detail the hydraulic characteristic measurements using LDV(Laser Doppler Velocimetry) in subchannels of a HANARO, KAERI research reactor, fuel bundle. The fuel bundle consists of 18 axially finned rods with 3 spacer grids and has a cylindrical configuration. Axial velocity and turbulent intensity were measured. The effects of the spacer grids on the turbulent flow were investigated using the experimental results. Pressure drops for each component of the fuel bundle were measured, and the friction factors of the fuel bundle and the loss coefficients for the spacer grids were estimated from the measured pressure drops. The turbulent thermal mixing phenomena were discussed.

1. Introduction

A research reactor with $30MW_{th}$, HANARO, is being operated at KAERI (Korea Atomic Energy Research Institute). The HANARO fuel bundle consists of 18 fuel elements(rods) which have eight axial rectangular fins on the outer cladding to enhance the heat transfer performance. Thus the fuel bundle is characterized by the presence of a number of axial fins on the cladding.

Much effort has been directed toward the study of LWR (Light Water Reactor) fuel bundles composed of bare rods [1-3] and FBR (Fast Breeder Reactor) fuel bundles composed of helically wire wrapped rods [4]. Compared with LWR and FBR fuel bundles, the study on the fuel bundles with axially finned rods is relatively scarce.

Grover and Venkat Raj [5] measured pressure drop for three different types of seven-rod bundles having axially finned rods. Their results showed that the friction factors for all of three types of rod bundles were less than those given by Moody' s curve for smooth tube of equivalent diameter.

Rowe et al. [6], Carajilescov and Todreas [7], Renksizbulut and Hadaller [8], and Vonka [9] performed experimental studies on bare rod bundle flows using LDV (Laser Doppler Velocimeter). Rowe et al., one of the earliest applications of LDV to subchannel flows, measured turbulent microscopic structures which were helpful in obtaining a better understanding of cross-flow mixing between neighboring subchannels. Their results showed that rod gap spacing was the most significant geometric

parameter affecting the flow structure. Decreasing the rod gap spacing increases the turbulence intensity, longitudinal macroscale, and the dominant frequency of turbulence. From the evaluation of the dominant frequency of turbulence, they suggested the presence of periodic flow pulsations in the gap region. Yang et al. [10] performed the turbulent measurement in an axially finned rod bundle without spacer grids. They observed turbulent flow characteristics in the developing and developed flow area. Their fuel elements were the same as those of the present study.

In this study, the detailed hydraulic characteristics were measured in subchannels of an axially finned rod bundles with spacer grids by using LDV. Axial velocity and turbulent intensity were measured. The effects of the spacer grids on the turbulent flow were investigated by the experimental results. Implications regarding the turbulent thermal mixing due to spacer grids were discussed. Pressure drops for each component of the rod bundle were also measured to estimate the friction factors in rod bundles and loss coefficients for the spacer grids.

2. Experimental Method

2.1. Test Fuel Bundle and Test Loop

A schematic diagram of the test loop is shown in Fig. 1. The test loop consists of a variable-speed motor pump, a water storage tank and a test section. Axial configuration of the test section with a test fuel bundle is shown in Fig. 2 including the components of the fuel bundle and pressure tap locations. The circular housing of the test section is made of an acrylic tube to provide access for laser beams to the location where the velocity measurement is to be preformed. The working fluid, water, flows upward through the test section and the flow rate is measured with a turbine flow meter. During the experiments the water temperature in the test section is measured with a

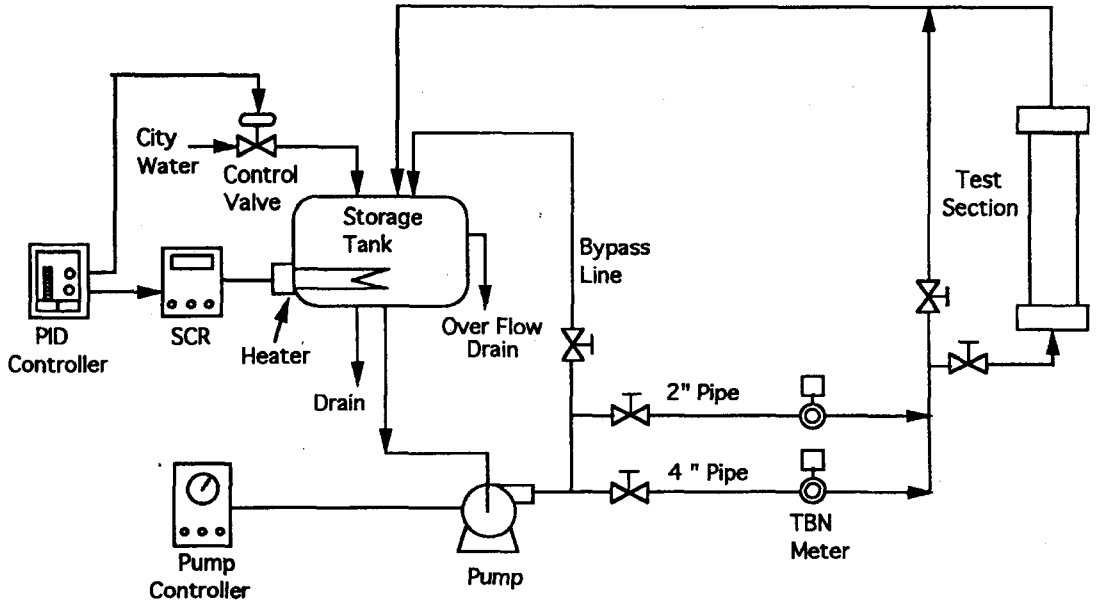

Fig. 1. Schematic Diagram of the Test Loop

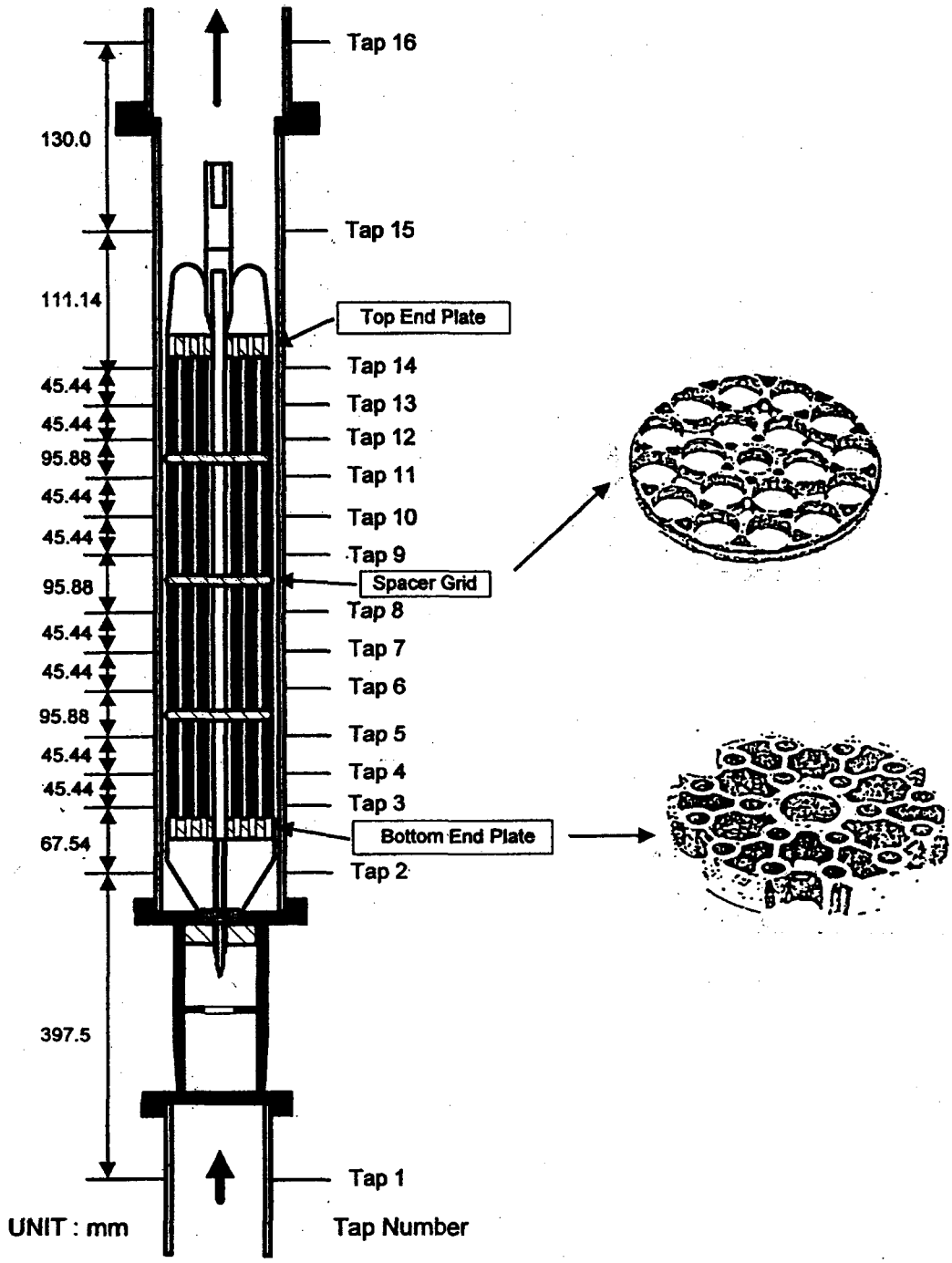

Fig. 2. Axial Configuration of the Rod Bundle with Spacer Grids

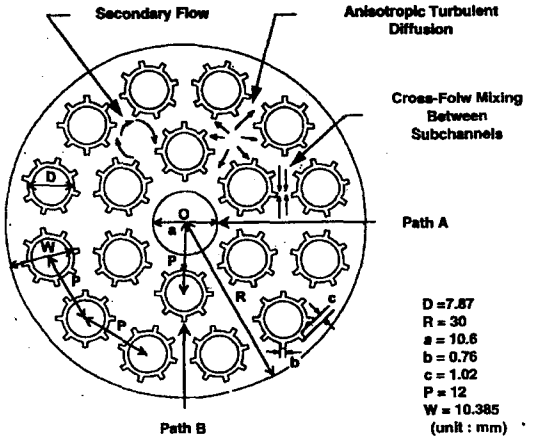

Fig. 3. Turbulent Phenomena in Subchannels

RTD (Resistance Temperature Detector) and maintained constant by a temperature control unit. A pressure transmitter and 8 differential pressure transmitters are used to measure the pressure and the pressure drop respectively. All these measuring parameters are gathered and processed with a data acquisition system.

The cross sectional view of the test section is illustrated in Fig. 3, which shows main dimensions and major turbulent phenomena in subchannels. The rods were arranged in a triangular and a square array with P/D =1.52, W/D =1.32.

During the experiment the water temperature was 40℃ and the flow rate varied from 5 to 16 kg/s, and in velocity measurement, the mean flow rate measured by the turbine flow meter was 12.7 kg/sec resulting in a bulk average flow velocity of 7.23 m/sec and Reynolds number based on hydraulic diameter, Re = 73000.

Experimental uncertainties in the measured quantities are evaluated according to the ANSI/ASME PTC 19.1 Code [20]. The accuracy of each instrument is used as a bias error and the precision error is evaluated from the standard deviation of the each measured parameter.

2.2. LDV (Laser Doppler Velocimeter)

The LDV measurement method is a non-intrusive optical technique with good spatial resolution, and is based on the principle that coherent laser light scattered from a particle moving with the flow experiences a Doppler frequency proportional to its velocity, *i. e.*, to the fluid flow velocity. The relationship between the Doppler frequency f_D and the velocity component perpendicular to the optical axis, $\tilde{u}$, is given by

$$f_D = 2\,\tilde{u}\,\sin\,\varkappa/\lambda \qquad (1)$$

, where λ is the laser wavelength and $\varkappa$ the half angle of the laser beam intersection. The one-component He-Ne LDV system(TSI 9100-3) was aligned by the dual-beam backward scattered mode for the present study. The dual-beam spacing is 50 mm and the focal -length of the focusing lens is 250 mm. Silicon carbide particles, 1.5μm in diameter, 3.2 g/cm^3 in density, 2.65 in refractive index, and 1.4 in geometrical standard deviation, were seeded into the fluid to obtain the scattered signal. The signals from the photomultiplier were processed using a counter type processor which consists of filters, an amplifier, a timer, a digital output, and a D/A (Digital to Analog) converter. The digital signals from the signal processor were used to obtain the turbulent velocity and intensity using the data analysis program FIND from TSI , in which the correcting process for velocity bias is included.

3. Results and Discussion

3.1. Pressure Drops

The pressure drops for each component of a fuel bundle were measured under various flow rate conditions. The pressure drop due to the spacer

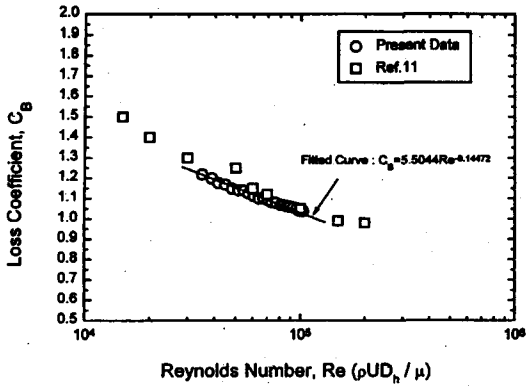

Fig. 4. Loss Coefficient of the Spacer Grid

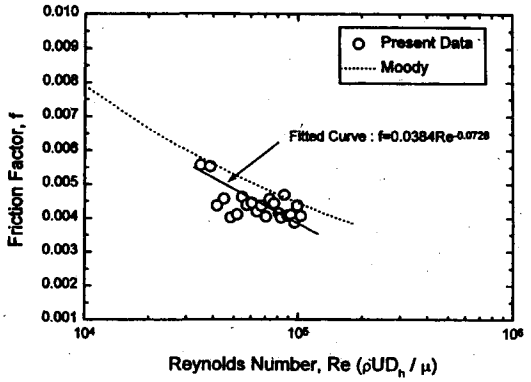

Fig. 5. Frication Factor for the Rod Bundle with Spacer Grid

grid (ΔP_G) is related to the bulk average fluid velocity, U_{av}, in the rod bundle.

$$\Delta P_G = C_B \rho \frac{U_{av}^2}{2} \quad (2)$$

, where C_B is the loss coefficient of the spacer and ρ the fluid density. Figure 4 shows the loss coefficients of the spacer grid and a fitted correlation curve of them. The loss coefficient was compared with that of the tube spacers axially connected in Ref. 11. Nearly same results have been observed in the two cases.

In Fig. 5, the friction factors in rod bundles were estimated from the measured pressure drops, and compared with Moody' s correlation for smooth tubes. The friction factors were calculated as

$$f = -\frac{dP}{dx}\frac{D_h}{2\rho U_{av}^2}. \quad (3)$$

The result shows that the friction factors for axially finned rod bundles are less than the values given by Moody' s curve, which coincides with the results of Grover and Venkat Raj [Type A in Ref. 5] on the flow in seven rod bundles with three axial fins, P/D = 1.224, and W/D = 1.047. The acceptable explanation about this trend in Fig. 5 can be given in Refs. 5 and 10. Comparing with the results for the case of fully developed flow in Ref. 10, the present values are a little more scattered. This may be attributed to the frictional distance between spacer grids.

Uncertainties of the loss coefficient and the friction factor are 2.8 and 3.4%, respectively.

3.2. Axial Velocity

Turbulent velocity measurements were performed at axial locations L/D_h = 2, 7, 14, and 23 for each grid span, and transversing Paths A(long path) and B(short path) (Fig. 3). Axial measuring length L is calculated from upper surface of each grid. Figure 6 shows the developing axial velocity profiles in each grid span at Path A(long path). The velocities are not fully developed in every grid span. The velocity profiles in the first grid span are different from those of other spans. However, beginning the second span, the velocity profiles develop in the same manner.

Figure 7 shows the developing axial velocity at Path B(short path) along the axial locations. In the first grid span, the velocity is not fully developed and the velocity profiles are different from those other spans, and starting the second grid span the velocity profiles show the same trend. This is due to the difference in shape between the bottom end

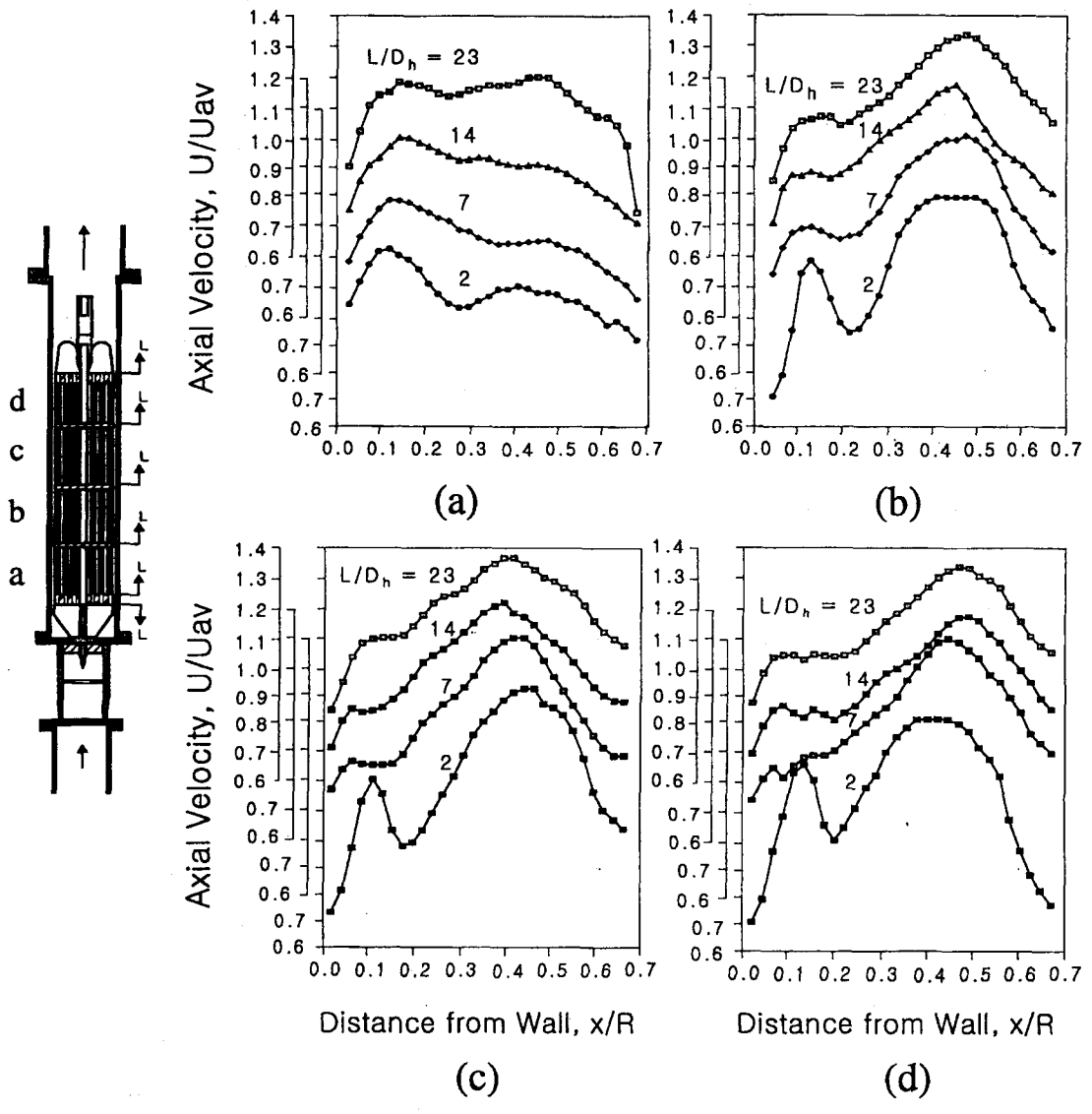

Fig. 6. Developing Axial Velocity at Path A

plate and the spcer grids. In Fig. 7, the velocity profiles near the grid, L/D_h = 2, are different from those of downstream locations. The velocity profiles become smooth as the flow develops, which is due to the flow mixing between subchannels.

The axial velocities near the wall at Paths A and B are plotted in Figs. 8 and 9 by wall coordinates and compared with the standard logarithmic equation,

$$U^+ = 2.44 \ln (y^+) + 5.0 \quad (4)$$

, and the logarithmic equation for the circular tube,

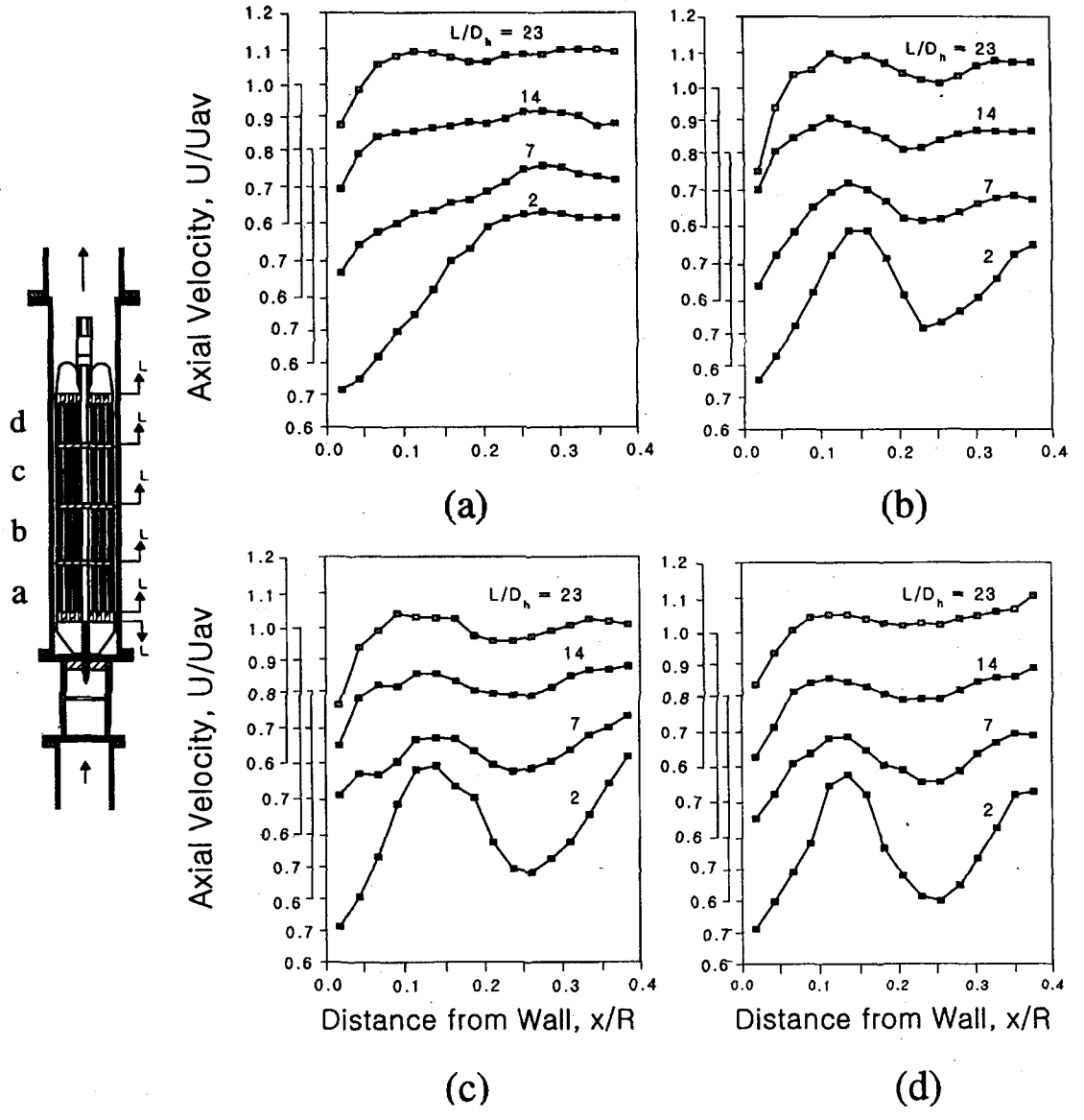

Fig. 7. Developing Axial Velocity at Path A

$$U+ = 2.50 \ln (y^*) + 5.5. \quad (5)$$

Most data are distributed under the two equations. This is due to the fact that flow is not fully developed but is in the developing region. As can be seen in Ref. 10 for the fully developed flow, the velocities are distributed over or between the two equations. For Path A, some data show the same trend as those of the fully developed flow. Because, it is assumed that the local shear stress in this geometry does not seriously deviate from the mean wall shear stress[12], and thus the friction velocity U^* in U^+, y^+ can be calculated from the measured pressure drop, dP/dx, as follows:

$$(U^*)^2 = \frac{\overline{\tau_w}}{\rho} = \frac{-D_h}{4\rho}\frac{dP}{dx} \quad (6)$$

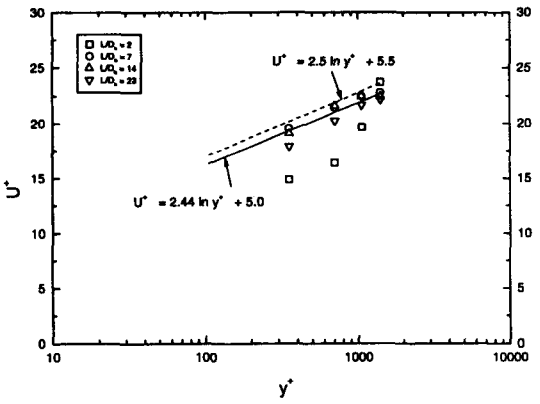

Fig. 8. Axial Velocity Profiles near Wall by Wall Coordinate at Path A

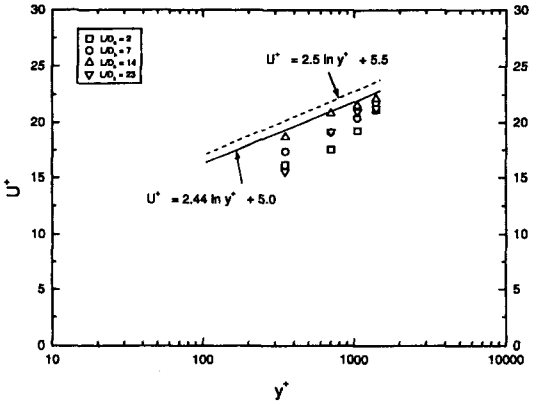

Fig. 9. Axial Velocity Profiles near Wall by Wall Coordinate at Path B

where $\overline{\tau}_w$ is the mean wall shear stress averaged along the perimeter of the rod bundle.

3.3. Axial Turbulent Intensity

Figure 10 represents the axial turbulent intensity in the first and third grid span at Path A with varying axial locations. The higher intensities are distributed at L/D_h = 2 near the lower spacer grid. The intensities decrease to the lowest values at L/D_h =23.

Axial turbulent intensities at Points 1-4 (Fig. 11) are shown in Fig. 12 as a function of axial locations. The higher turbulent intensities are observed immediately downstream of the bottom end plate and at each spacer grid, and they decay rapidly to the stable values. Axial turbulent intensity distributions are repeated in nearly the same manner for each spacer grid span.

The turbulent intensity decay can be explained with turbulent decay in turbulent flows through mesh grids or screens [13]. Axial turbulent intensity decay in each grid span for the present work is shown in Figs. 13-16. Usually the turbulent decay rate is expressed as

$$\frac{\overline{u^2}}{U^2} = \alpha\ (x/M - x_0/M)^{-n} \qquad (7)$$

, where α, M, and x_0 are the fitting constant, the grid mesh size, and the virtual origin, respectively. Grid mesh size M is assumed to be the pitch length, P in the present study. In Figs. 13-16, the turbulent intensity decay for each grid span was compared with the correlation obtained by Yang and Chung [13] for the downstream region of the spacer grids for PWR 5X5 rod bundle,

$$\frac{\overline{u^2}}{U^2} = 0.04\ (x/P)^{-1.2}. \qquad (8)$$

In Figs. 13~16, the turbulent intensity decay current for the present study (finned rod bundle) is some different from the case of PWR rod bundle (bare rod bundle). The values for the case of the present study level out more rapidly than for the case of the PWR 5×5 rod bundle. This implies that the flow mixing occurs more actively in the finned rod bundle than in the bare rod bundle. The difference in the decay current between the first grid span and the other spans may be due to the difference in shape in them.

3.4. Implications Regarding Turbulent Thermal Mixing

Thermal hydraulic behavior of the fluid at the

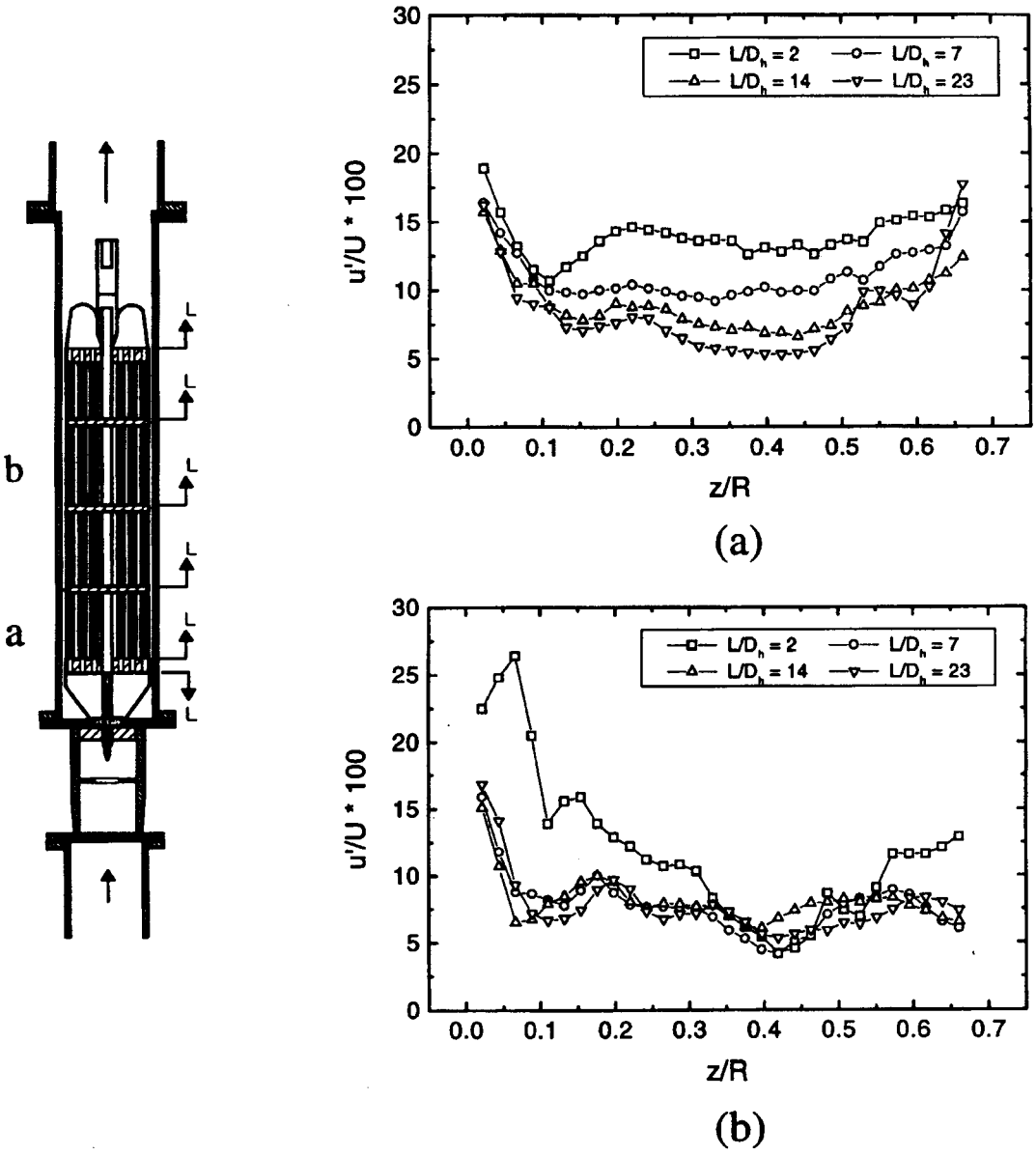

Fig. 10. Axial Turbulent Intensity for the Rod Bundle with Spacer Grid at Path A

spacer grid is hard to analyze in detail due to the complex geometry of the grid. To approach this problem, the relationship between heat and momentum transfer in turbulent flow was used to get information on the thermal behavior near the spacer grid.

Yao *et al.* [14] studied heat transfer augmentation by straight grid spacers in rod bundles. For single phase flow and for post-critical heat flux dispersed flow, the local heat transfer at a straight spacer and at its upstream and downstream locations were investigated. The

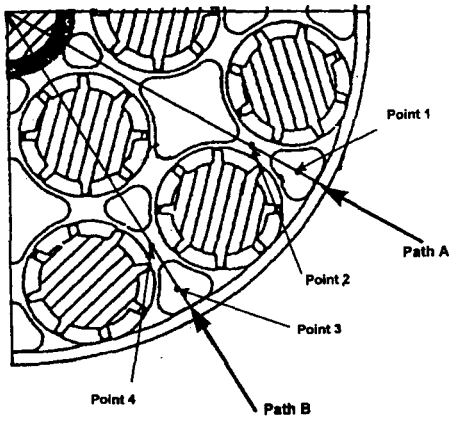

Fig. 11. Meausring Point of Turbulence Decay

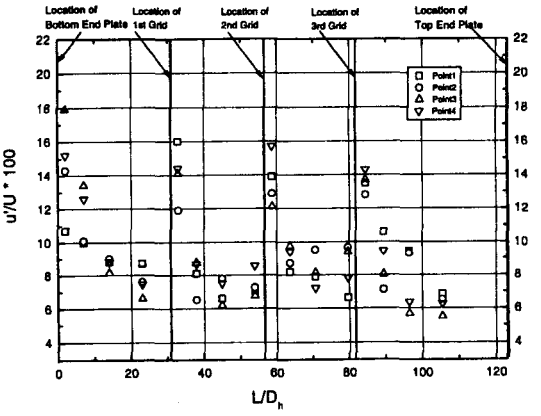

Fig. 12. Axial Turbulent Intensity Decay

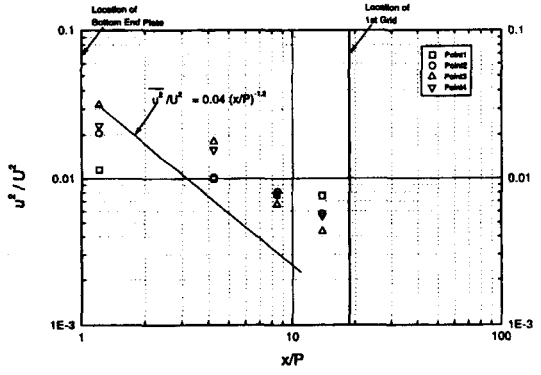

Fig. 13. Axial Turbulent Intensity Decay Downstream of the Bottom End Plate

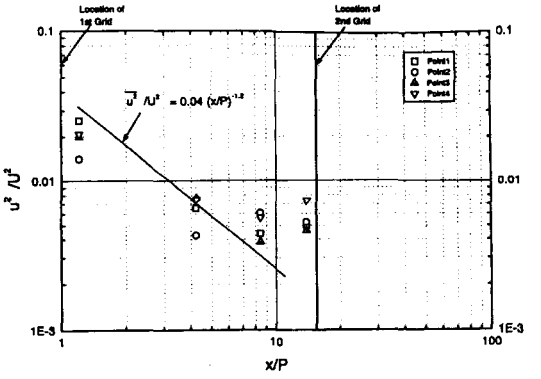

Fig. 14. Axial Turbulent Intensity Decay Downstream of the 1st Spacer Grid

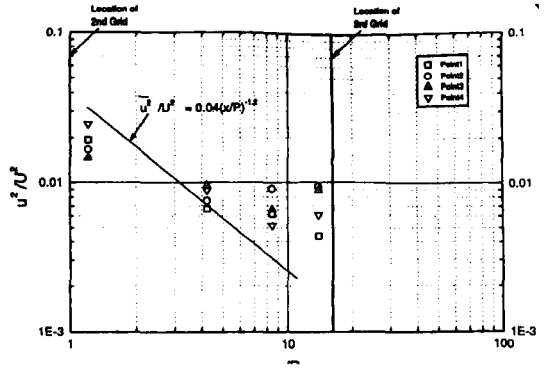

Fig. 15. Axial Turbulent Intensity Decay Downstream of the 2nd Spacer Grid

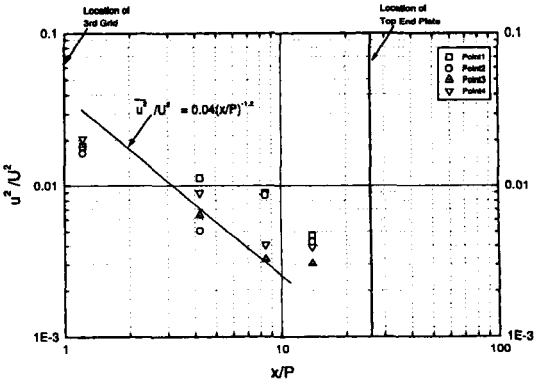

Fig. 16. Axial Turbulent Intensity Decay Downstream of the 3rd Spacer Grid

highest local heat transfer was observed near the spacer grid, and downstream of the spacer grid. The heat transfer augmentation rapidly decayed exponentially with x/D_h.

In the present study, some quantitative values of turbulent thermal mixing which significantly contributes to the heat transfer augmentation near spacer grid were evaluated as follows. The lateral thermal energy exchanges at a gap are based on a fluctuating mass exchange between neighboring subchannels. The heat transfer through the gap per unit length can be expressed as

$$q_{ij} = m_{ij}' c_p (T_i - T_j) \tag{9}$$

, where T_i, T_j and m_{ij}' are the bulk temperatures of two adjacent subchannels i and j, and the fluctuating cross-flow mixing rate per unit length between subchannels, respectively. m_{ij}' is defined by Stewart *et al.* [15]

$$m'_{ij} = \rho\, w_{eff}\, s \tag{10}$$

, where w_{eff} and s are the effective mean mixing velocity and rod gap spacing, respectively. If the enthalpies and velocities of the neighboring subchannels are different, an exchange of energy and momentum flux will occur. The expressions for the net turbulent energy flux, F_h, and momentum flux, F_m, between subchannels can be given, respectively, by (Stewart, *et al.* [15])

$$F_h = \rho\, w_{ef} \Delta h, \tag{11}$$

and

$$F_m = F_t\, \rho\, w_{eff}\, \Delta U \tag{12}$$

, where Δh and ΔU are the average enthalpy and axial velocity difference between subchannels, and F_t is a correction factor which is related to the difference between turbulent energy and momentum transport. The turbulent cross-flow flux can be expressed as diffusive energy flux between centroids of subchannels. And by introducing a mixing factor [16-18], it can be given as

$$F_h = \varepsilon\, Y \rho\, \Delta h/\Delta y \tag{13}$$

, where ε, Y and Δy are the reference turbulent eddy viscosity, a mixing factor, and a centroid or mixing distance between subchannels, respectively. Ingesson and Hedberg [19] used the eddy viscosity at the center of a circular tube as a reference eddy viscosity, *i. e.*,

$$\varepsilon = \nu(f_{Dt}/8)^{0.5}\, Re/20 \tag{14}$$

, where f_{Dt} and ν are the friction factor of a circular tube and the kinematic viscosity of a fluid, respectively. Equating Eq. (11) to Eq. (13) yields

$$Y = w_{eff}\, \Delta y/\varepsilon \tag{15}$$

Möller [16] obtained the mixing velocity by supposing that the dominant frequency eddies were responsible for the turbulent mass flow exchange between the gaps. However, since w_{eff} is not available in the present measurement, $w_{eff} \fallingdotseq u'$ was assumed at the central region in the gap. Local mixing factor nondimensionalized by Y_0, which is the local value in the fully developed flow region without spacer grid, is shown in Fig. 17.

Y_0 was assumed from the results of Yang *et al.* [10]. As shown in Fig. 17, the mixing factors have the highest values at the

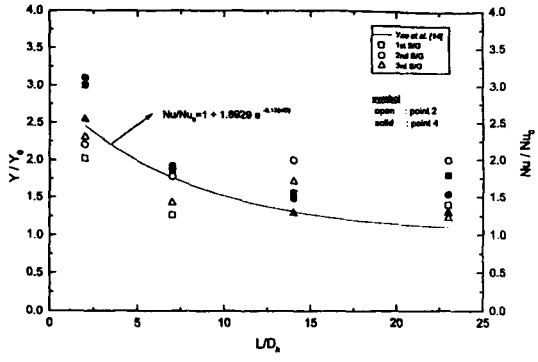

Fig. 17. Local Mixing Factor Downstream of the Spacer Grid

immediate downstream of the spacer grids, and beyond this region the values reach nearly the same level. This means that turbulent mixing occurs actively in the immediate downstream region of each spacer grid, and beyond this region the mixing occurs steadily. Local heat transfer rate predicted by using the correlation of Yao *et al.* [14] shows nearly the same qualitative tendency.

Uncertainties of the average velocity(U), the turbulent intensity, and the mixing factor are 2.9, 11, and 8.5%, respectively.

4. Concluding Remarks

This study measured the detailed hydraulic characteristics in subchannels of axially finned rod bundle with spacer grids. The experimental results led to the following conclusions:

The friction factors for the axially finned rod bundle used in this study are less than those given by Moody' s correlation for smooth tube of equivalent diameter.

The velocity profiles are not fully developed in the flow subchannels. The velocity profiles in the downstream span of the bottom end plate are different from those of other spans. However, starting the second span, the velocity profiles develop in the same manner.

The axial turbulent intensity is highest immediately downstream of each grid, and decays to a stable level as the flow develops. Turbulent intensity decay rates can be explained by grids turbulence decay.

The turbulent mixing occurs actively in immediate downstream region of each spacer grid, and beyond this region the mixing occurs steadily. Local heat transfer rate shows nearly the same qualitative tendency.

Nomenclature

c_p	specific heat, kJ/kg℃
D	rod diameter, m
D_h	hydraulic diameter, m
F_h	net turbulent energy flux, J/m2s
F_m	momentum flux, kg/ms2
F_t	correction factor
f_D	Doppler shift frequency, 1/s
h	enthalpy, J/kg
Δh	enthalpy difference between subchannels, J/kg
L	axial length, m
P	pitch, m
Re	Reynolds number
s	rod gap spacing
U	axial time mean velocity, m/s
U^*	friction velocity (= $\sqrt{\tau_w/\rho}$), m/s
U^+	nondimensional velocity in wall coordinate (=U/U^*)
$\tilde{u}$	instantaneous velocity , m/s
u	axial fluctuating velocity, m/s
u'	rms value of u, m/s
U_{av}	channel bulk average velocity, m/s
W	wall distance, m
x	axial coordinate, m
Y	mixing factor
y	traversing distance from wall (y=z), m
y^+	nondimensional distance from wall in

	wall coordinate ($=yU^*/\nu$)
Δy	centroid or mixing distance between subchannels, m
z	coordinate of traversing direction, m

Greek Symbols

ϵ	turbulent eddy viscosity, m^2/s
$\varkappa$	half angle of laser beam intersection, degree
λ	laser wave length, m
ν	kinematic viscosity, m^2/s
ρ	fluid density, kg/m^3

References

1. K. Rehme, "Distribution of Velocity and Turbulence in a Parallel Flow Along an Asymmetric Rod Bundle," *Nuclear Technology*, **15**, 148 (1982)
2. K. Rehme, "The Structure of Turbulent Flow Through Rod Bundles," *Nucl. Engrg. Des.* **99**, 141 (1987)
3. J. D. Hooper, and K. Rehme, "Large - scale Structural Effects in Developed Turbulent Flow Through Closely-Spaced Rod Arrays," *J. Fluid Mech.* **145**, 305 (1984)
4. J. J. Lorenz, and T. Ginsberg, "Coolant Mixing and Subchannel Velocities in an LMFBR Fuel Assemblies," *Nucl. Engrg. Des.*, **40**, 315 (1977)
5. R. B. Grover, and V. Venkat Raj, "Pressure Drop Along Longitudinally Finned Seven-Rod Cluster Nuclear Fuel Elements," *Nucl. Engrg. Des.* **58**, 79 (1980)
6. D. S. Rowe, B. M. Johnson, and J. G. Knudsen, "Implications Concerning Rod Bundle Cross-flow Mixing Based on Measurements of Turbulent Flow Structure," *Int. J. Heat Mass Transfer*, **17**, 407 (1974).
7. P. Carajilescov, and N. E. Todreas, "Experimental and Analytical Study of Axial Turbulent Flows in an Interior Subchannel of a Bare Rod Bundle," *J. of Heat Transfer, Trans. of the ASME*, **101**, 354 (1979).
8. M. Renksizbulut, and G. I. Hadaller, "An Experimental Study of Turbulent Flow Through a Square Array Rod Bundle," *Nucl. Engrg. Des.* **91**, 41 (1986).
9. V. Vonka, "Measurement of Secondary Flow Vortices in a Rod Bundle", *Nucl. Engrg. Des.* **106**, 191 (1988).
10. S. K. Yang, M. K. Chung and H. J. Chung, "Measurements of Turbulent Flow in Axially Finned Rod Bundles," Experimental Thermal and Fluid Science, **5**, 828 (1992).
11. K.Rehme, "Pressure Drop Correlations for Fuel Element Spacers" , *Nuclear Technology*, **17**, 12 (1973).
12. K.Rehme, "Personal Communication", (1991)
13. S. K. Yang, and M. K. Chung, "Turbulent Flow through Mixing Spacer Grids in Rod Bundles" , *National Heat Transfer Conference*, **14**, 33 (1995).
14. S. C. Yao, L. E. Hochreiter and W. J. Leech, "Heat Transfer Augmentation In Rod Bundles near Spacer Grids", *J. of Heat Transfer, Trans. of the ASME*, **104**, 76 (1982).
15. C. W. Stewart et al., COBRA-IV : the Model and the Method", Battele, Pacific Northwest Laboratories (1977).
16. S. V. M ller, "Single-phase Turbulent Mixing in Rod Bundles", Experimental Thermal and Fluid Science, **5**, 26 (1992).
17. K. Rehme, "The Structyre of Turbulence in Rod Bundles and the Implication s on Natural Mixing between the Subchannels", Int. J. Heat Mass Transfer, **35**, 567 (1992).
18. X. Wu and A. C. Trupp, " Spectral Measurements and Mixing Correlation Simulated Rod Bundles Subchannels", *Int. J. Heat Mass Transfer*, **37**, 1277 (1994).

19. L. Ingesson and S. Hedberg, "Heat Transfer between Subchannels in a Rod Bundles", *Heat Transfer, Vol. III, Fc.7.11* (1970).
20. ANSI/ASME PTC 19.1, "ASME Performance Test Codes : Supplement on Instruments and Apparatus, Part-1 ; Measurement Uncertainty" (1985).